https://doi.org/10.48048/tis.2023.6478

Impact of Surrounding Gas Density on the Turbulent Liquid Jet

Muhamad Said[1,*], Abouelmagd Abdelsamie[1,2], Kareem Emara[1] and Momtaz Sedrak[1]

[1]Department of Mechanical Power Engineering, Faculty of Engineering at Elmataria, Helwan University, Cario, Egypt
[2]Laboratory of Fluid Dynamics and Technical Flows, Otto von Guericke University Magdeburg, Magdeburg, Germany

([*]Corresponding author's e-mail: muhamad.said@m-eng.helwan.edu.eg)

Received:12 December 2022, Revised: 27 January 2023, Accepted: 7 February 2023, Published: 18 March 2023

Abstract

This numerical study aims to investigate the impact of surrounding gas density on liquid turbulent jet. Incompressible large eddy simulations (LES) with Wall-Adapting Local Eddy-Viscosity (WALE) sub-grid scale model in ANSYS-FLUENT were performed to capture the morphology of the breakup as well as the important flow field characteristics. A volume of fluid (VOF) approach was used to track the unsteady evolution and breakup of the liquid jet. Different variables have been examined to assess this impact. These variables are instantaneous velocity, liquid volume fraction, and turbulent kinetic energy. Also, the centerline values have been investigated to obtain the jet half-width and spray dispersion angle. The jet diameter and exit velocity are 0.2 mm and 100 m/s, respectively. Three different liquid-to-gas density ratios of 54.03, 32.42 and 23.49 are considered, corresponding to ambient gas density of 15, 25 and 34.5 kg/m^3, respectively. It has been found that the jet speed and the liquid core length are inversely proportional to the density of the ambient gas. Regarding the liquid core length, it was noted that the effect of gas density on the liquid core length is considerably stronger in the gas density range between 15 - 25 kg/m^3 (corresponding to density ratios of 54.03 - 32.42) than that in the range of 25 - 34.5 kg/m^3 (corresponding to density ratios of 32.42 - 23.49). The results, also, showed that increasing the gas density leads to an increase in Weber number, which in turn causes a high instability, that makes the breakup initiates closer to the nozzle exit and occurs with higher rate. Likewise, it has been found that the jet width and the spray dispersion angle increase with increasing the gas density.

Keywords: Spray, Turbulent jet, LES, Spray dispersion angle

Introduction

Fluid turbulence characterization coming out of a simple orifice is very important in engineering because of its many applications, such as: combustion, thermal spray, agriculture, inkjet, coating, medical sprays and much more [1]. Atomization of a turbulent jets is an integral part of the study of turbulent liquid jet and a basic concept for physical modeling tools development to predict the spray characteristics. The process of turning the liquid jets into droplets, which is called disintegration. The process of turning the column into droplets, which is called milk, increases the liquid surface area, and thus increases the transfer of both mass and heat between the liquid and the surrounding fluid. And here lies the spray importance of spray in the different applications [2]. Atomization study is undoubtedly fundamentally important process, and at the same time very difficult and challenging because it is unsteady and complex for the highest degrees, and this is due to its involvement of different types of instabilities [3,4].

Over the past years, the scientific community has been very interested in describing the behavior of cylindrical liquid jets discharging into a quiescent gaseous atmosphere. The first experimental investigation was recorded in the first half of the 19th century [5]. When liquid is discharging from a circular opening, it is producing a cylindrical jet. The liquid discharging rate from the orific is a key factor in the mechanisms of disintegration. The plot of the jet breakup length as a function of the orific exit bulk velocity, which called stability curve, is the common way of categorizing the disintegration mechanisms of cylindrical jets [6-9]. Breakup length is the coherent part of the jet, i.e., it is the length of the continuous jet connected to the nozzle [10].

Hiroyasu and Kadota [11] deduced an experimental relationship between pressure of the fuel injection, the density of ambient air, the mass flow ate of the fuel and the droplets sauter mean diameter (SMD). Elkotb [12], Varde *et al.* [13] and Faeth *et al.* [14], In the following years, studied additionally the

effects of the density and viscosity of the liquid and the surface tension. Moreover, an empirical relationship of breakup length of the liquid core was derived by Reitz and Bracco [15]. implosion of cavitation bubbles, turbulence in the liquid jet and aerodynamic liquid-gas interaction were identified, by Fath *et al.* [16], as the most dominant liquid jet atomization mechanism.

Gupta *et al.* [17] studied experimentally the primary atomization of evaporating laminar liquid jets of *n*-pentane and *n*-heptane emerging from a circular nozzle into high-temperature turbulent coflows of air in confined pipe. Their results in the near-field region of the injector nozzle showed that the length of the liquid jets formed increases with the fuel injection velocity and decreases with the air velocity. They also found that the smaller droplets were formed at higher velocities of fuel and air. Furthermore, they observed, within their investigated range of conditions, that the jet length and droplet size are not affected by the air inlet temperature.

The atomization effect on entrainment in the gas phase of a 2-phase free jet, as a function of the mixing ratio, was investigated by Hotz *et al.* [18] at ambient conditions. They used the tracer gas (helium) concentration in the gas phase to indicate the local mixing ratios for 3 different nozzles by applying 5 different gas-to-liquid ratios (GLR) for the 2-phase free jet as well as a single-phase free jet.

The liquid preheating impact on primary jet breakup in a coaxial twin-fluid injector was investigated by Kumar and Sahu [19]. Recorded shadow-graphic images of 3 different jets, with different injection temperatures, taken by high speed camera were analyzed to measure several parameters such as the jet breakup length. It was found that preheating the jet to a medium temperature has a very strong effect on the breakup process of the jet.

As the mechanisms of cavitation bubbles implosion and liquid jet turbulence were related to phenomena inside the nozzle, many researchers studied the extent to which the breakup length of the liquid jet was affected by the flow inside the nozzle. For example, Martínez-Martínez *et al.* [20] concluded that the nozzle diameter is an important factor affecting the penetration length. Furthermore, Suh and Lee [21] concluded that the fuel atomization and the cavitation bubble generation in the nozzle could be enhanced by increasing the ratio of the length of the nozzle to its width. Sirignano and Mehring [22] summarized many reviews about the results and studies related to the main fields related to the physics of liquid jet disintegration.

When focusing carefully on aforementioned literature, you can notice that the process of atomization has been ignored, especially the part of primary step. Not only that, but also the part about atomization analysis was just a correlation developed between spray characteristics and specific parameters such as: nozzle dimensions, injection pressure, liquid properties, etc. This is because of the inability of the experimental methods in specific importance diagnostics. Some diagnostics were developed later to obtain these characteristics by experiments. These diagnostics were mentioned in [23-25]. Following this development and other, rapid changes has occurred in recent decades concurrently with the emergence of new experimental Technologies. We should take advantage of this development in making more effort to study and investigate the part that was neglected in the past, i.e., the primary step of the atomization process, which is the main link between the liquid jet discharging from the nozzle and the fully developed spray [10,26].

From the numerical point of view, over the years, huge efforts have been made to simulate the breakup process of a jet of liquid with several methods. These numerical studies were mainly based on solving Navier-Stokes equation which was accompanied by appropriate interface capturing method such as volume of fluid (VOF) [27], level set method [28] or a combination of both [29,30]. Selection of the appropriate method from them depends on the advantages and disadvantages of each method for each application separately, and it varies from one problem to another.

Among these numerical studies, research focused on the effect of the flow inside the nozzle on the breakup process of the jet. To name a few, Som *et al.* [31] solved the Reynolds-Averaged Navier-Stokes (RANS) equations to simulate the nozzle flow only. They analyzed the mass flow at the exit orifice of the nozzle as a function of injection pressure, the position of the needle left and the fuel type. Yuan and Schnerr [32], after that, perform RANS simulations to combine the in-nozzle flow with the discharged liquid jet. They studied 2 jet atomization cases, one of them include the cavitation phenomenon while the other was without the cavitation for the purpose of comparing the 2 cases for enhancing the atomization process. Furthermore, at recent times, Ghiji *et al.* [33] resolves LES for in-nozzle flow and the following atomization, using simplifying nozzle. They found a compatible results with that obtained experimentally during the Diesel injection initial stages. After that, Xiao *et al.* [34] resolved the jet flow approach without the flow inside the nozzle. On the other hand, the evaluation of the in-nozzle swirl effect on the flow field of annular gas-liquid jets was studied by Siamas *et al.* [35] using detailed VOF simulations. They reported that central recirculation region was developed as a result of the swirling motion. Grosshans *et al.* [36]

showed that the range of liquid-gas density ratio from 10 to 30 have a small effect on the aerodynamic breakup. Also, they reported that if the liquid gas viscosity ratio was reduced from 7 to 1, then the droplet will get smaller and thus the dispersion angle will get larger.

Shinjo and Umemura [37] discussed the physical mechanisms including ligament and droplet formation that still need further investigations, where they studied the primary atomization of liquid injected at high speed into still air to elucidate physical processes by direct numerical simulation (DNS).
Zhang *et al.* [38] studied the effect of the angle between the central liquid (glycerol/water mixture with a high dynamic viscosity of 200 mPa.s) jet and the annular airflow on the primary atomization process of coaxial, twin-fluid nozzle. They observed that increasing the angle from 0 to 30 ° promotes the breakup of the jet, increases the flow velocity of the gas phase close to the liquid jet and decreases its core length. However, further increase of the angle from 30 to 60 ° leads to a decreased gas flow velocity along the liquid jet and an increase of core length.

In an unconventional work, Leng *et al.* [39] simulated, using (VOF-LES) method, the multi-phase flow inside and outside the spirally grooved hole (SGH) nozzle to investigate its influence on the behavior of breakup process and cavitating flow characteristics for diesel nozzles. They found that the inner-hole's spiral grooves added more dynamics besides aerodynamic effects for the breakup of liquid jets which in turn led to strong enhancement of the emerging jet breakup and substantially near-field dispersion angle.

Recently, Abdelsamie and Thévenin [40], by means of DNS, quantified the impact of shear on evaporation and spray autoignition mechanisms by comparing droplets evolving in a high-speed jet flow or in a nearly quiescent environment. Also, the impact of local equivalence ratio, droplet diameter and jet velocity were investigated by varying these parameters. They revealed in their results that the temporally-evolving jet is a promising numerical configuration to study spray-turbulence interaction, evaporation, mixing, and auto-ignition mechanisms. They observed, also, that the autoignition delay time is strongly dependent on the droplet diameter and jet velocity, while it is far less sensitive to the equivalence ratio.

Motivation and contributions of the proposed work

From the literature reviewed in the previous section, it can be concluded that the most important parameters to be studied in the liquid turbulent jet are, the velocity, nozzle diameter, and the liquid-to-gas density ratio. Even though, lot of research studied these parameters, there are several ranges, to the author knowledge, are still not covered. The present study tries to cover the missing ranges. Therefore, in this article, the impact of surrounding gas density on 0.2 mm diameter liquid turbulent jet was investigated. Incompressible-LES approaches [41] with WALE sub-grid scale model [42] in ANSYS-FLUENT were performed to capture the morphology of the breakup as well as the important flow field characteristics. A volume of fluid (VOF) approach [27] was used to track the unsteady evolution and breakup of the liquid jet. For jet exit velocity is 100 m/s, 3 different liquid-to-gas density ratios of 54.03, 32.42, and 23.49, corresponding to ambient gas densities of 15, 25 and 34.5 kg/m^3, respectively, were considered.

This article organized as follows: The employed mathematical models are reviewed in the next section, includes the applied LES method and the VOF model. Then the employed geometry, meshing, boundary conditions, and solvers are discussed in detail. After that, mesh dependency test and validation of turbulence and multiphase models are introduced. Then the results of the investigation of the impact of the changing of gas density on the turbulent jet behavior were discussed. At the end, conclusions are provided.

Mathematical models

In this section, the employed governing equations will be briefly summarized, where the applied LES method and the Wall-Adapting Local Eddy-Viscosity (WALE) model which used as Subgrid-scale model are explained.

LES method is a very promising approach for the simulation of turbulent flows because computation times are significantly lower than those of DNS. Further, their resolution of turbulent structures is more accurate in comparison to RANS simulations [33]. The LES method is commonly used in the study of turbulent flows in which large scales of motion are resolved and the effect of small scales is modeled with the help of a sub-grid scale (SGS) model which usually employs an eddy viscosity assumption to model the SGS stress.

The Wall-Adapting Local Eddy-Viscosity (WALE) model, which imployed in the present work because it overcomes the limitations of the Smagorinsky model [41], uses a specific velocity scale for the calculation of eddy viscosity which enables it to predict accurate values in the regions of high vorticity as well as high irrotational strain [43]. The governing equations can be summarized as following.

The instantaneous local variable is divided, based on the filter, to resolvable scale variable $\bar{\varphi}_i$, and subgrid-scale one $\acute{\varphi}_i$:

$$\varphi_i = \bar{\varphi}_i + \acute{\varphi}_i \tag{1}$$

The filtered equations are developed from the incompressible Navier-Stokes equations of motion:

$$\frac{\partial u_i}{\partial t} + u_j \frac{\partial u_i}{\partial x_j} = -\frac{1}{\rho}\frac{\partial p}{\partial x_i} + \frac{\partial}{\partial x_j}\left(\upsilon \frac{\partial u_i}{\partial x_j}\right) \tag{2}$$

where the u_i, p, and υ are the i-th velocity component, pressure and kinematic viscosity of fluid flow, respectively. Using the decomposition of Eq. (1) for velocity and pressure, then filtering Eq. (2) gives the equations of motion for the resolved flow field as follows:

$$\frac{\partial \bar{u}_i}{\partial t} + \bar{u}_j \frac{\partial \bar{u}_i}{\partial x_j} = -\frac{1}{\rho}\frac{\partial \bar{p}}{\partial x_i} + \frac{\partial}{\partial x_j}\left(\upsilon \frac{\partial \bar{u}_i}{\partial x_j}\right) + \frac{1}{\rho}\frac{\partial \tau_{ij}}{\partial x_i} \tag{3}$$

The extra term $\frac{\partial \tau_{ij}}{\partial x_i}$ in Eq. (3) represents the divergence of SGS stress tensor, arises from the non-linear advection terms, due to the fact that:

$$\overline{u_j \frac{\partial \bar{u}_i}{\partial x_j}} \neq \bar{u}_j \frac{\partial \bar{u}_i}{\partial x_j}, \tag{4}$$

hence the SGS stress tensor,

$$\tau_{ij} = \overline{u_i u_j} - \bar{u}_i \bar{u}_j \tag{5}$$

Similar equations can be derived for the subgrid-scale field. Subgrid-scale turbulence models usually seek to calculate the SGS stress using the following assumption:

$$\tau_{ij} - \frac{1}{3}\tau_{kk}\delta_{ij} = -2\rho \upsilon_t \bar{S}_{ij} \tag{6}$$

The isotropic part of the subgrid-scale stresses τ_{kk} is not modeled but added to the filtered static pressure term. $\bar{S}_{ij}$ is the rate-of-strain tensor for the resolved scale defined by:

$$\bar{S}_{ij} = \frac{1}{2}\left(\frac{\partial \bar{u}_i}{\partial x_j} + \frac{\partial \bar{u}_j}{\partial x_i}\right), \tag{7}$$

and υ_t is the kinematic turbulence viscosity. Substituting into the filtered Navier-Stokes Eq. (3):

$$\frac{\partial \bar{u}_i}{\partial t} + \bar{u}_j \frac{\partial \bar{u}_i}{\partial x_j} = -\frac{1}{\rho}\frac{\partial \bar{p}}{\partial x_i} + \frac{\partial}{\partial x_j}\left([\upsilon + \upsilon_t]\frac{\partial \bar{u}_i}{\partial x_j}\right), \tag{8}$$

In Eqs. (2) - (8), the incompressibility constraint has been used to simplify the equation. Then the pressure is modified to include the trace term $\tau_{kk}\delta_{ij}/3$, where the δ_{ij} is the Kronecker delta. In the WALE model the eddy viscosity is calculated by:

$$\mu_t = \rho L_S^2 \frac{(S_{ij}^d S_{ij}^d)^{3/2}}{(\bar{S}_{ij}\bar{S}_{ij})^{5/2} + (S_{ij}^d S_{ij}^d)^{5/4}} \tag{9}$$

where,

$$L_s = C_w V^{1/3}, \tag{10}$$

$$S_{ij}^d = \frac{1}{2}\left(\bar{g}_{ij}^2 + \bar{g}_{ji}^2\right) - \frac{1}{3}\delta_{ij}\bar{g}_{kk}^2, \tag{11}$$

$$\bar{g}_{ij} = \frac{\partial \bar{u}_i}{\partial x_j}, \tag{12}$$

$$\bar{g}_{ij}^2 = \bar{g}_{ik}\bar{g}_{kj} \tag{13}$$

where, the constant $C_w = 0.325$, and V is the volume of the computational cell.

Numerical settings

The employed geometry, meshing, boundary conditions, and solvers are discussed in detail in this section. Where the work here is divided into 2 stages; first stage is the validation and mesh dependency stage, while the second stage is a parametric study. In the second stage, the impact of the gas density will be analyzed.

Geometry and meshing

In this work, because of the limited computational resources 2-dimensional simulation was performed in a domain with dimensions of 40*D*×13*D*, where *D* is the jet diameter (jet width in 2D) as it illustrated in the schematic diagram in **Figure 1**. The boundary condition, as illustrated in **Figure 1**, are velocity inlet boundary conditions at the edges number 1 and 2, and pressure outlet at edges number 3 and 4. First of all, the employed model and domain are validated with the work of Pavlović *et al.* [44]. The validation has been performed by comparing the current work at 4 different mesh size with that of Pavlović *et al.* [41]. The 4 cases M1, M2, M3, and M4 are summarized as in **Table 1**. The mesh is a structured equidistance quad-cells with cell size of D/10 (10 μm), D/13 (7.7 μm), D/30 (3.3 μm) and D/50 (2 μm), leads to total number of elements of 52 000, 87 880, 468 000, 1 300 000 for Cases M1, M2, M3, and M4, respectively. Where the diameter of the jet in these cases is 0.1 mm.

Table 1 Mesh specifications.

	M1	**M2**	**M3**	**M4**
Element size	*D*/10 (10 μm)	D/13 (7.7 μm)	D/30 (3.3 μm)	D/50 (2 μm)
Number of elements $N = (N_y \times N_x)$	130×400 = 52,000	169×520 = 87,880	390×1200 = 468,000	650×2000 = 1,300,000

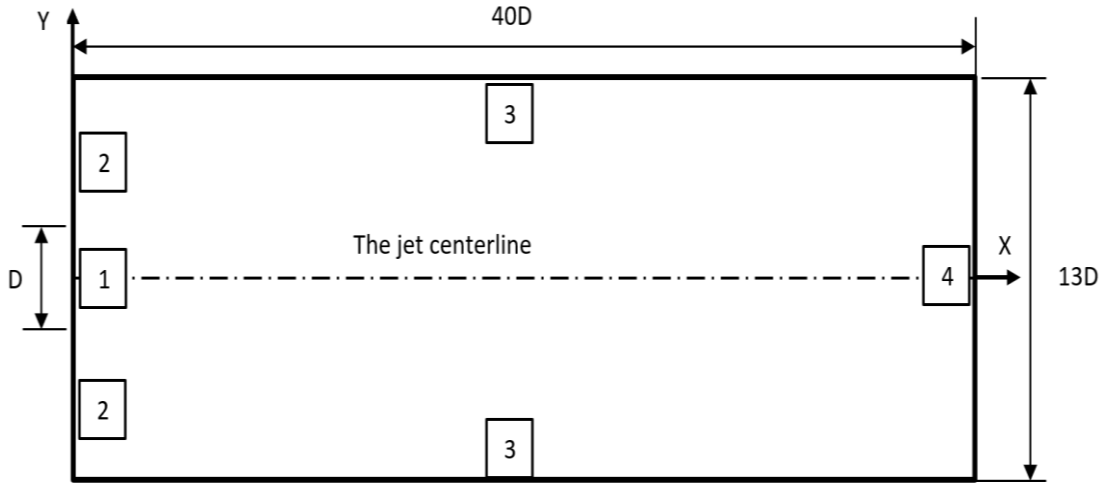

Figure 1 Schematic diagram of the dimensions of computational flow domain and boundary conditions.

Numerical setups and models

Ansys-Fluent 2019 R3 was used in this work for all simulations with the following settings.

1) Solver: Pressure-based solver, absolute velocity formulation, transient (unsteady) simulation, 2D domain.

2) Multiphase model: Volume of fluid (VOF) model, 2 Eulerian phases [domain (gas) –injection (liquid)], implicit volume fraction formulation, sharp interface modeling type and implicit body force formulation.

3) Phase interaction: Continuum surface force as a surface tension force modeling with constant surface tension coefficient of 0.0264 N/m.

4) Turbulence model: LES with WALE subgrid-scale model.

5) Working fluids: Diesel as a liquid phase, and air as a gas phase.

6) Boundary conditions: As it is shown in **Figure 1**, velocity inlet (Neumann boundary condition) and pressure outlet (Dirichlet atmospheric pressure),

7) Initial conditions: the initial conditions are summarized in **Table 2**. Where in this table, the U_e and U_r are exit liquid jet velocity and relative velocity between the liquid jet and ambient gas, respectively. The turbulence intensity $I = 0.16\mathrm{Re}^{-1/8}$ as it is recommended by Abdelsamie and Thévenin [40].

8) Time step: 6×10^{-8}, 3×10^{-8} and 2×10^{-8} s used for the case at different jet velocities of 50, 100 and 150 m/s, respectively, to keep Courant-Friedrichs-Lewy (CFL) number smaller than 0.5.

Table 2 Initial conditions used for the validation case and the parametric study part.

	Validation part	**Present study**
Exit jet velocity, $\boldsymbol{U_e}$, (m/s)	50, 100, 150	100
Diameter (jet width in 2D) $\boldsymbol{D}$, (mm)	0.1	0.2
Liquid density, $\boldsymbol{\rho_l}$, (kg/m^3)	810.5	810.5
Liquid dynamic viscosity, $\boldsymbol{\mu_l}$, (kg/m.s)	1.54×10^{-3}	1.54×10^{-3}
Surface tension, $\boldsymbol{\sigma}$, (N/m)	0.0264	0.0264
Liq. Weber Number, $\boldsymbol{We_l = \frac{\rho_l U_r^{\,2} d}{\sigma}}$	7675, 30701, 69077	61402
Reynolds number, $\mathrm{Re} = \frac{\rho_l U_e d_j}{\mu_l}$	2631, 5263, 7894	10526
Turbulence intensity $[\boldsymbol{I}] = \boldsymbol{0.16\mathrm{Re}^{-1/8}}$ (%)	5.98, 5.48, 5.21	5.03
Gas density, $\boldsymbol{\rho_g}$ (kg/m^3)	34.5	15, 25, 34.5
Gas dynamic viscosity, $\boldsymbol{\mu_g}$, (kg/m.s)	1.54×10^{-5}	1.54×10^{-5}
Gas Weber Number, $\boldsymbol{We_g = \frac{\rho_g U_r^{\,2} d}{\sigma}}$	327, 1307, 2940	1136, 1894, 2614

Mesh dependency and validation

Mesh dependency test has been performed by using 4 mesh resolution levels as described (Section: **Geometry and meshing)**; from coarse to fine. Conditions similar to that of Pavlović *et al.* [44] is selected in the validation and mesh dependency stage as it is summarized in **Table 2**. **Figure 2** show the volume fraction of the liquid at time $t = 6$ μs obtained from the simulation at different mesh sizes (M1, M2, M3, and M4) compared with reference case from Ref. [44]. As it can be observed from **Figure 2**, the volume fraction at Case M1, is completely different than that from the reference case. It is very obvious that the large cell size is not enough to capture the liquid breakup and shear layer in appropriate manner. With decreasing the cell size, the volume fraction structure approaches that of the reference case, especially for Cases M3 and M4.

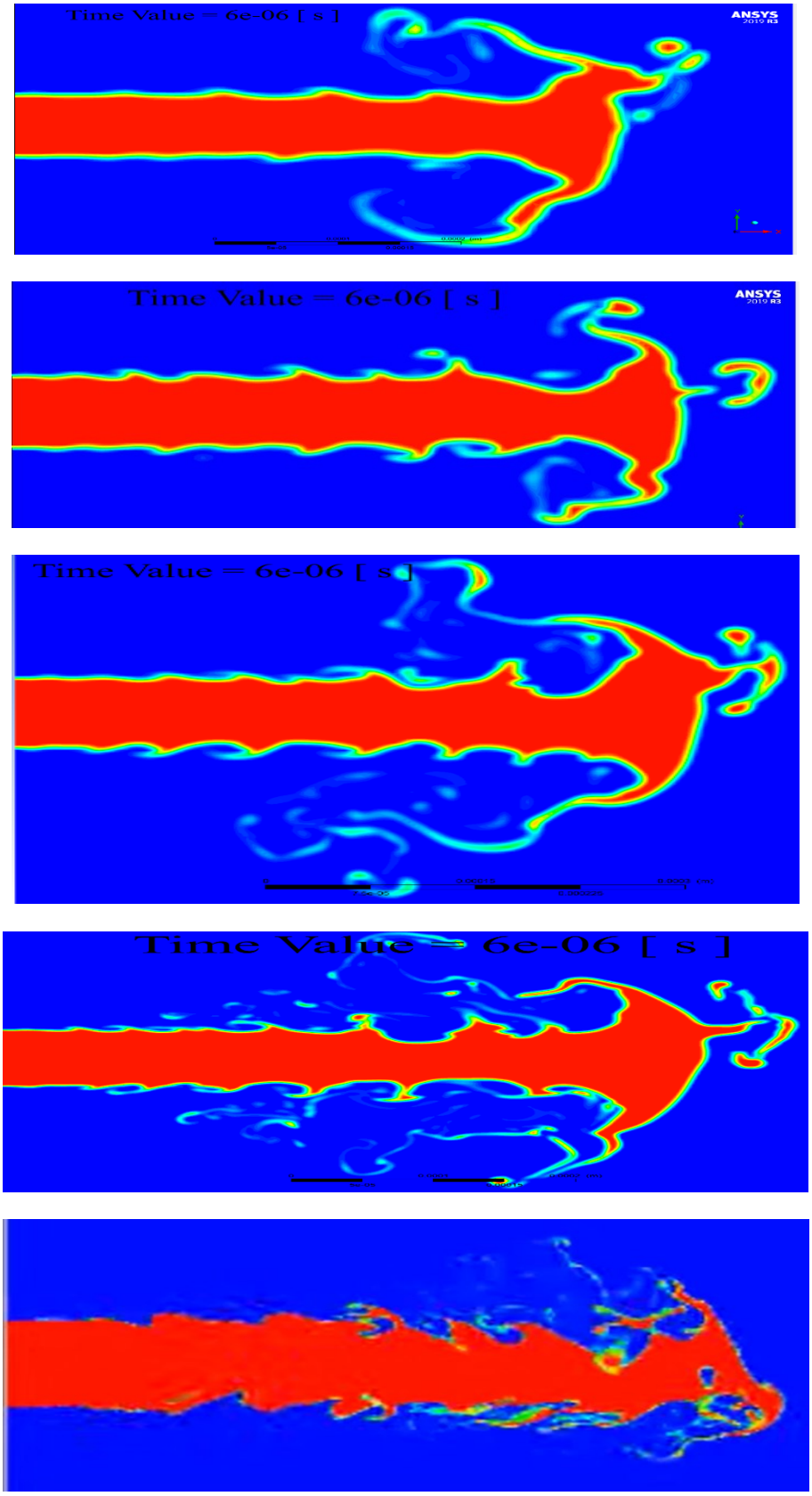

Figure 2 Volume fraction of the liquid jet at time of 6 μs at jet velocity of 100 m/s. The cases from top to bottom are M1, M2, M3, M4, and reference case from by Pavlovic *et al.* [44].

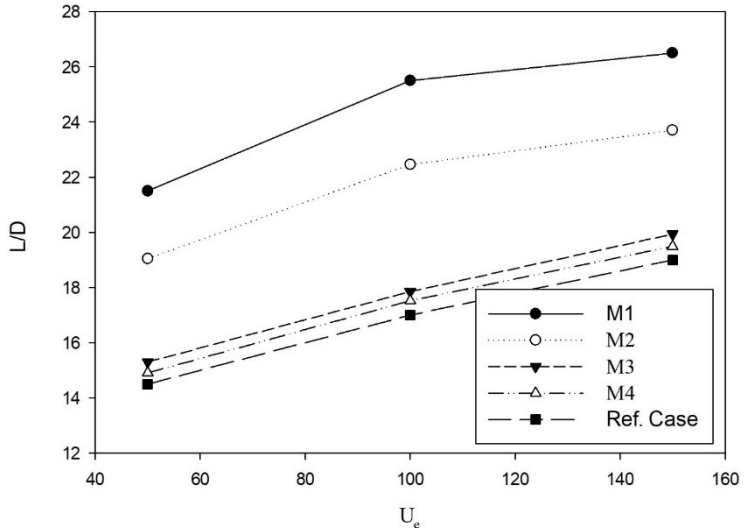

Figure 3 Liquid core length obtained from the present simulation at different cell size (M1, M2, M3, and M4) and the result of Pavlovic *et al.* [44] and at different jet injection velocities (50, 100, 150 m/s).

This can be confirmed more precisely from computing the liquid core length, according to the definition of Pavlović *et al.* [44], at different jet exit velocity. The computed liquid core length at jet exit velocities of 50, 100 and 150 m/s for the different mesh sizes and the reference case is shown in **Figure 3**. With these results, it is confirmed that the Cases M3 and M4 show accepted agreement with that of the reference case. As a conclusion and based on the available resources, the cell size of the Case M3 will be employed in the rest of this work.

Results and discussion

After validating the employed models and finishing the mesh dependency test, the impact of the changing of gas density on the turbulent jet behavior will be investigated. Three values have been used for the gas density ρ_g = 15, 25 and 34.5 kg/m^3. This leads to liquid-to-gas density ratios of 54.03, 32.42, and 23.49, respectively. In this section, color contours of instantaneous and average values of velocity and kinetic energy will be explained. Temporal-average of line cuts, downstream growth of the jet half-width, and average volume fraction also will be considered. The last part of the result section will show the points that having liquid volume fraction (LVF) value of 0.05.

Instantaneous contours

In this section, 3 important variables will be visualized as an instantaneous value to discuss the impact of the changing the gas density on the instantaneous flow field at consecutive time steps. These variables are streamwise velocity u (**Figure 4**), liquid volume fraction (**Figure 5**), and turbulence kinetic energy (**Figure 6**), respectively.

As it is expected, increasing the gas density would lead to high resistance in the way of the liquid jet. This makes the liquid penetration is more difficult. Looking at the instantaneous contour in **Figure 4**, the liquid jet core reaches the end of the domain faster in the gas with lower density (**Figure 4** left) compared to the other 2 cases. Therefore, increasing the gas density decelerates the jet speed.

The effect of increasing the ambient gas density on the liquid jet breakup obeys another scenario. Where increasing the density of the gas, increases the gas Weber number. This cause a high instability which leads to more breakup at higher gas density as it can be seen from the last column in **Figure 5**. This instability initiates the breakup earlier and closer to the nozzle exit; and with higher rate, while the case with smaller gas density has less breakup. In **Figure 5**, it is clear that the most amount of disintegrated ligaments from the jet surface and then breakup droplets is found more in the case with larger gas density.

The turbulent kinetic energy is presented in **Figure 6**. As a consequence of the jet instability in the case of larger gas density, and due to the stronger shear layers and jet breakup, the turbulence kinetic energy expected to be found at higher gas density case. Where smaller ligaments have higher inertial which leads to higher kinetic energy. This emphasizes that smaller liquid-to-gas density ratio leads to more breakup.

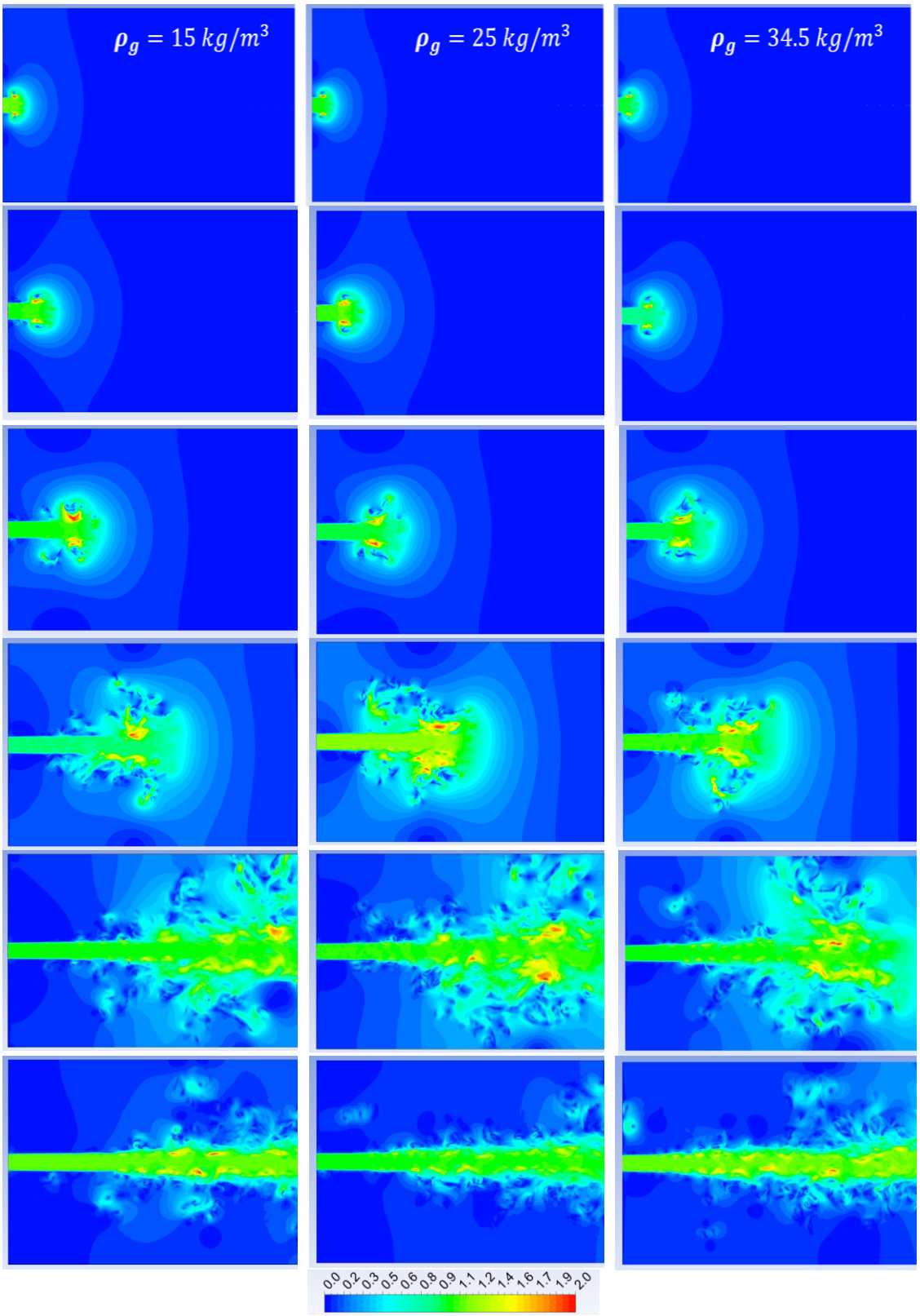

Figure 4 Instantaneous normalized streamwise velocity, u/U_e , at times, from top to bottom, $t = 3, 6, 12, 24, 48, 96\ \mu s$.

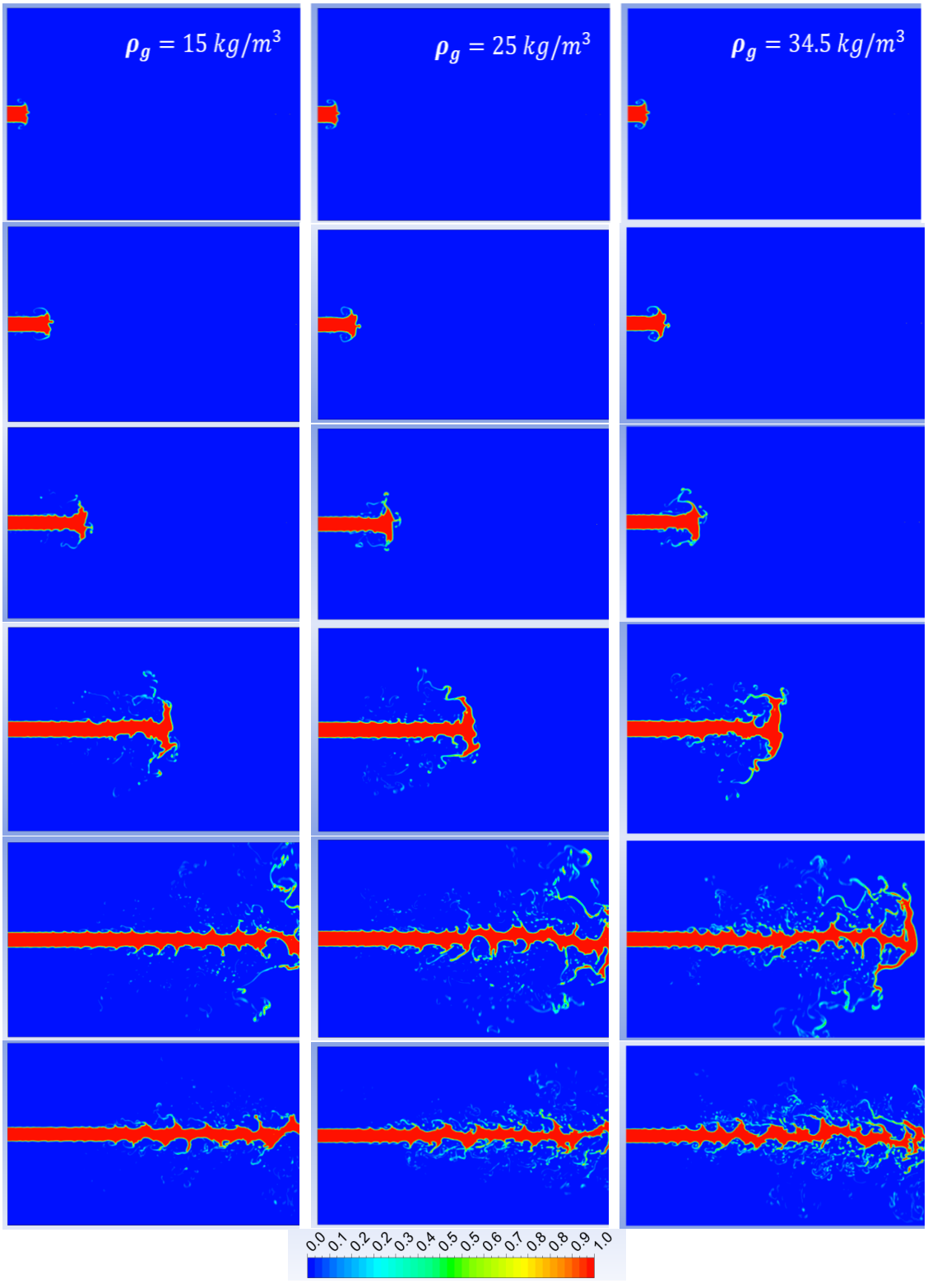

Figure 5 Instantaneous liquid volume fraction at times, from top to bottom, $3, 6, 12, 24, 48, 96\ \mu s$.

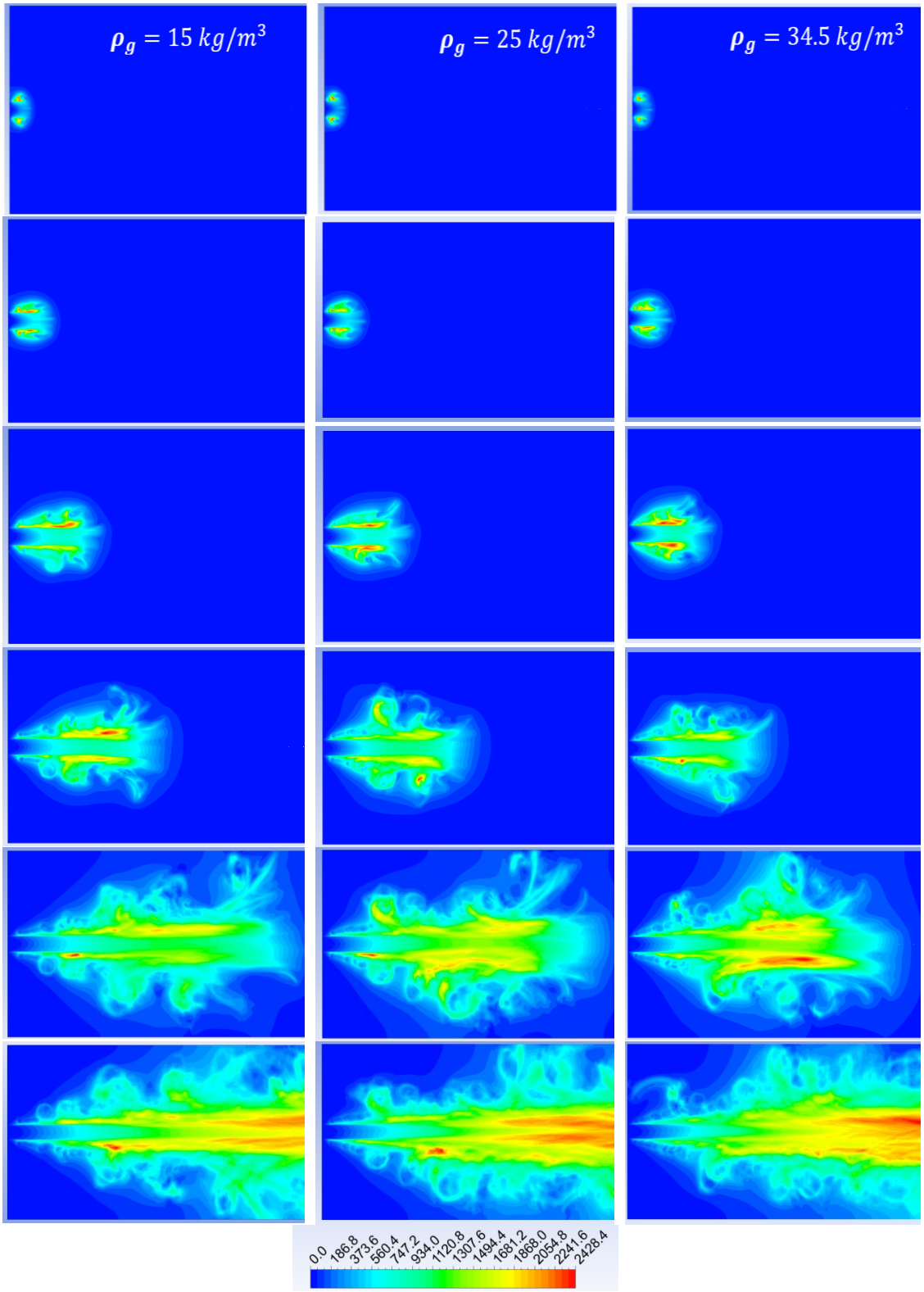

Figure 6 Instantaneous turbulent kinetic energy, in units $[J/kg]$, at times, from top to bottom, $t = 3, 6, 12, 24, 48, 96\ \mu s$.

Average contours

Contours of temporal-averaged normalized streamwise velocity u_{avg}/U_e are shown in **Figure 7(a)**. The potential core preservation distance was noted in this figure. It was also depected that there is a progress from no interaction to a gradual interaction of the liquid jet with the surrounding fluid. It has been observed that the jet width increases as the gas density increase.

The average liquid volume fraction contours illustrated in **Figure 7(b)**. The potential core preservation length noted in this figure as well, where the liquid core length decreases with increasing ambient gas density. Also, overall sight of the dispersion intensity of disintegrated ligaments and droplets from the jet surface, represented in the prevalence of the non-zero volume fraction points in the domain, can be noted from **Figure 7(b)**. It is found that the dispersion increases with increasing ambient gas density. This can be discussed in terms of spray dispersion angle as it will be analyzed in the next section. The figure indicates that the dispersion angle increases with the gas density as it will be confirmed in the next section.

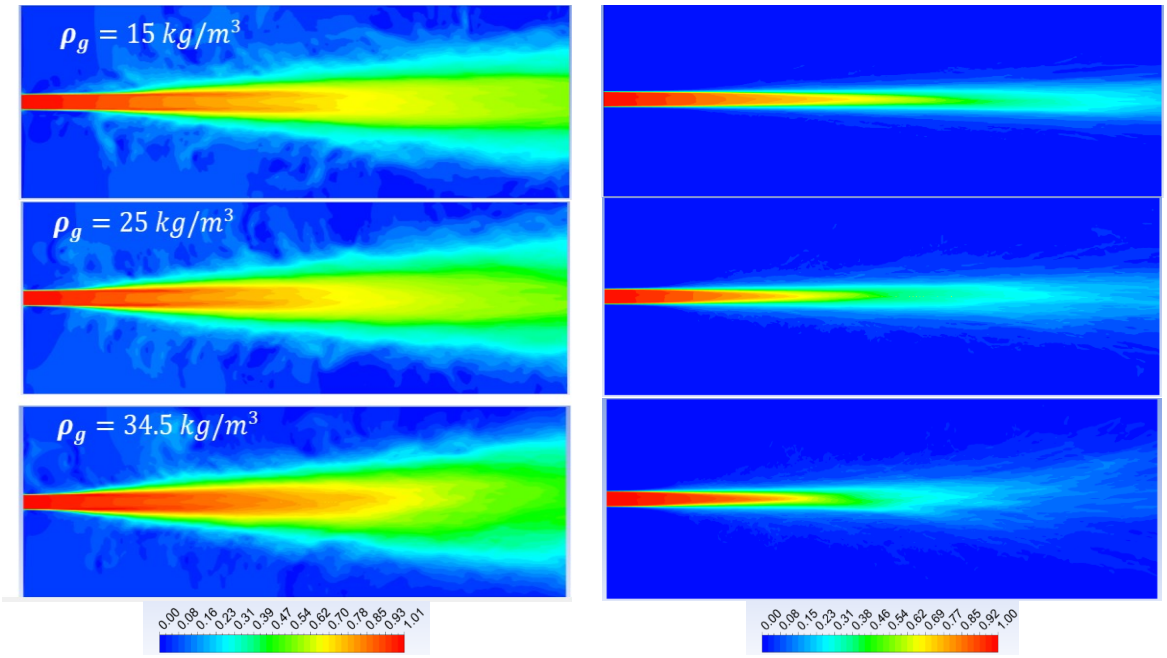

(a) (b)

Figure 7 Contours of temporal-averaged quantities at different gas densities. (a) average normalized streamwise velocity, u_{avg}/U_e, and (b) average liquid volume fraction.

Centerline average values

Figure 8(a) shows the decay of temporal-averaged normalized streamwise velocity, u_{avg}/U_e, along the jet centerline. It is clear that the decay is the same in the 3 cases (ρ_g= 15, 25 and 34.5 kg/m^3) up to 20D apart from the nozzle exit, then the jet in the case with highest gas density shows the strongest decay, while the jet in the lowest gas density shows the weakest decay.

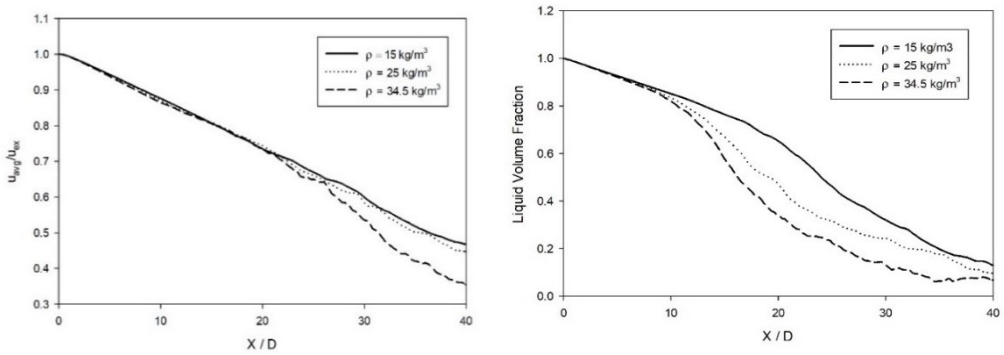

(a) (b)

Figure 8 Centerline cut of temporal-average of (a) streamwise velocity and (b) liquid volume fraction.

Figure 8(b) shows the average liquid volume fraction which used to determine the potential core preservation length as mentioned in previous section. It is found that the liquid core length is 24D, 19.1D and 16.2D at gas density of 15, 25 and 34.5 kg/m^3, respectively. It is very clear that, the effect of gas density on the liquid core length is considerably stronger in the gas density range between 15 - 25 kg/m^3 than that in the range of 25 - 34.5 kg/m^3. This observation agrees with that observed by Arai *et al.* [46] and Hiroyasu *et al.* [47]. It can be concluded that the increasing the gas density enhances the Kelvin-Helmholtz instabilities of the jet.

Values at x-distances from the jet exit

Figure 9 shows the normalized average streamwise velocity in the radial direction at x-distance of 5D, 15D, 25D, and 35D from the jet exit. This figure is used to determine the jet width, according to the definition of Stanley *et al.* [48], at the mentioned distances for different gas densities.

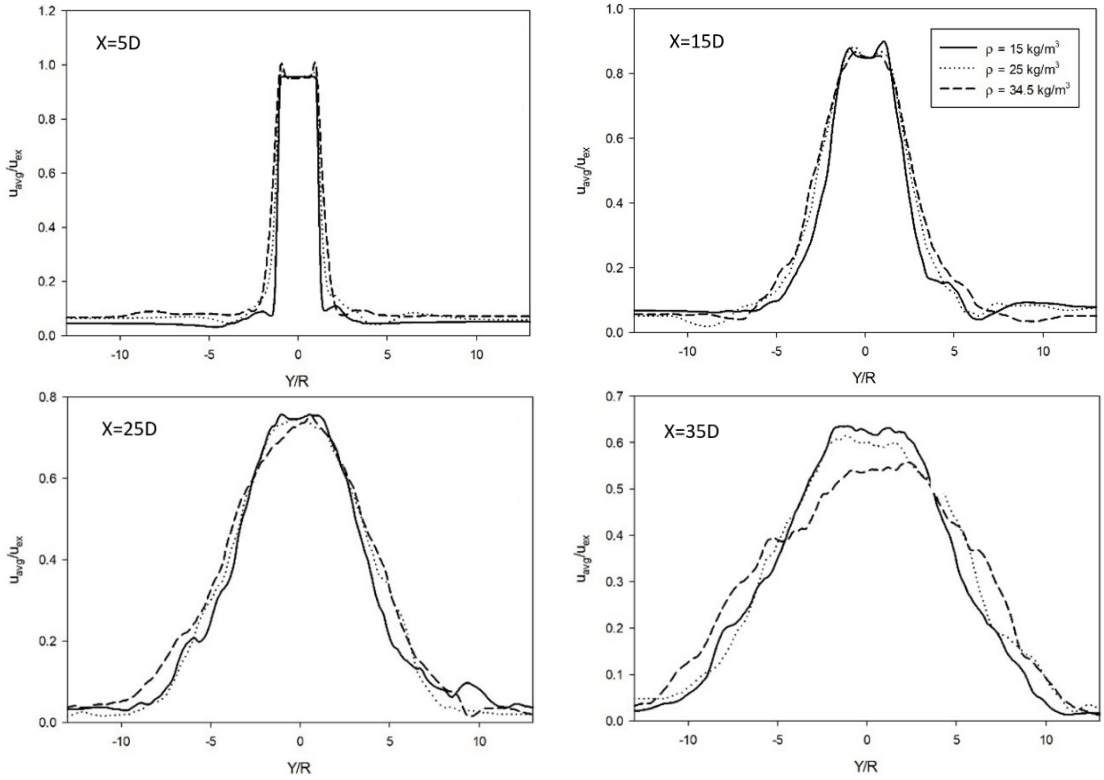

Figure 9 Temporal-averaged normalized streamwise velocity at different x-locations.

The width of the jet is expressed as the half-width, $Y_{0.5}$, defined as the distance from the jet centerline to the point at which the average streamwise velocity is half of the centerline average streamwise velocity. From this figure, it is very clear that that the jet width increases with the gas density and with the distance apart from the jet exit. **Table 3** represents the values of centerline normalized average streamwise velocity and the jet half-width at the x-distances that obtained from **Figure 9**. It can be observed from **Table 3** that the half-width of the evolving jet is not linearly proportional to the gas density (or liquid-to-gas density ratio). However, the half-width is linearly proportional to the distance from the nozzle exit.

Table 3 Centerline temporal-averaged normalized streamwise velocity and normalized jet half-width at different axial locations for the 3 tested cases.

ρ_g (kg/m^3)	u_{cl}/u_e				$Y_{0.5}/D$			
	5D	**15D**	**25D**	**35D**	**5D**	**15D**	**25D**	**35D**
15	0.955	0.848	0.748	0.63	1.18	2.44	3.84	5.3
25	0.954	0.846	0.738	0.602	1.34	2.86	4.26	6.1
34.5	0.951	0.851	0.734	0.538	1.5	3.1	4.7	7.7

The growth of the jet half-width is presented in **Figure 10**, which demonstrates that the jet width increases with increasing the ambient gas density. The behavior trend of the relation between jet width and the distance from the jet is consistent with the observation of Stanly *et al.* [48].

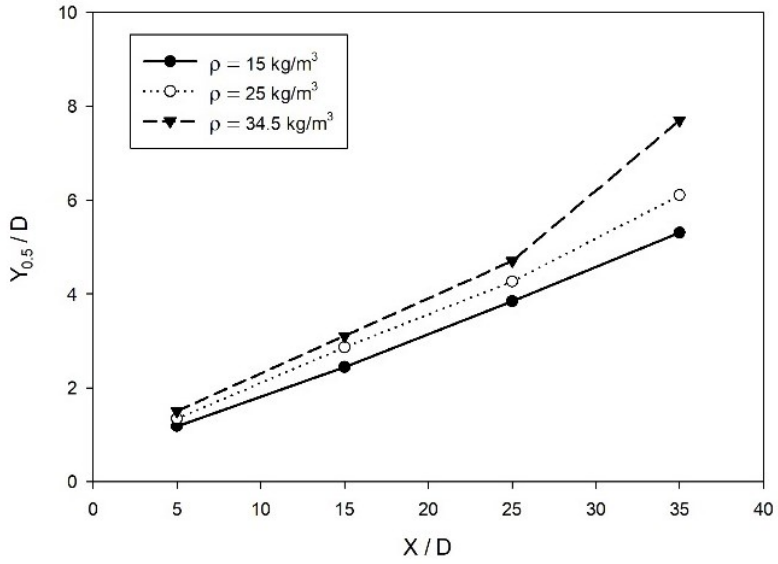

Figure 10 Downstream growth of the jet half-width.

Figure 11 shows the average liquid volume fraction in radial direction at X/D equal 5, 15, 25 and 35 for the 3 gas densities. As mentioned above, the values of spray dispersion angles can be determined using this figure after defining how to predict its value.

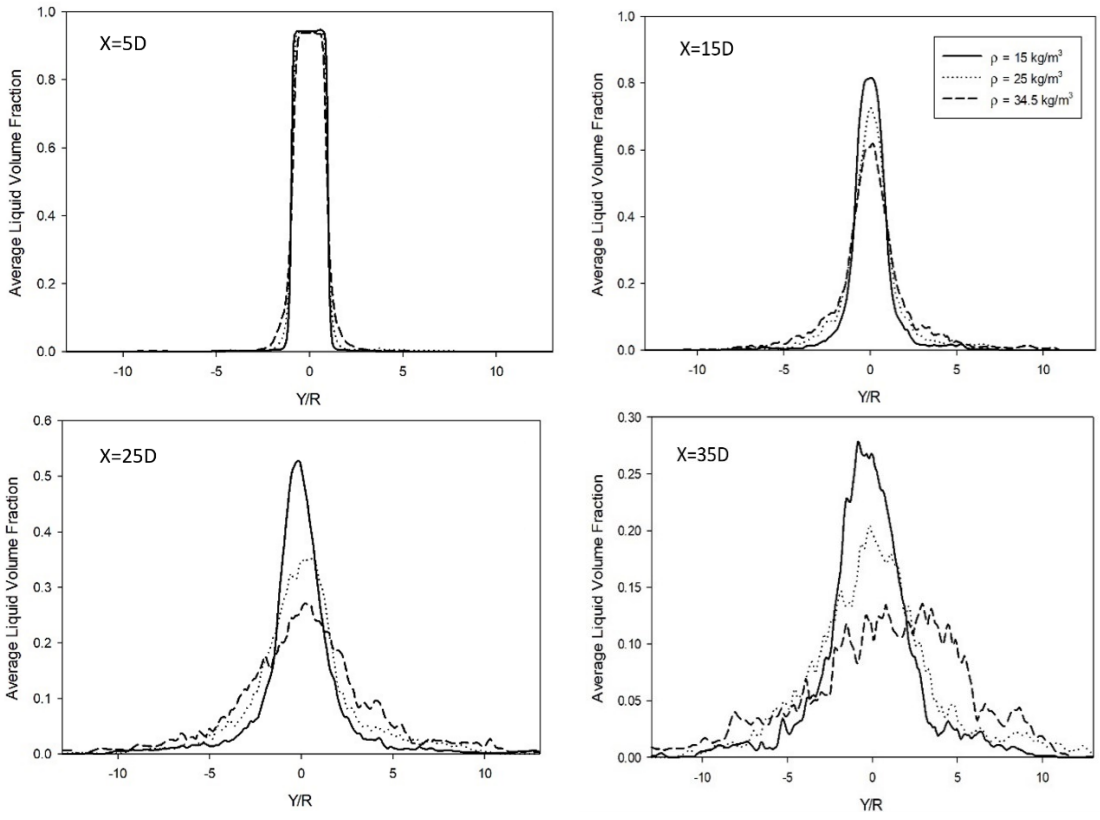

Figure 11 Average liquid volume fraction at different x-locations.

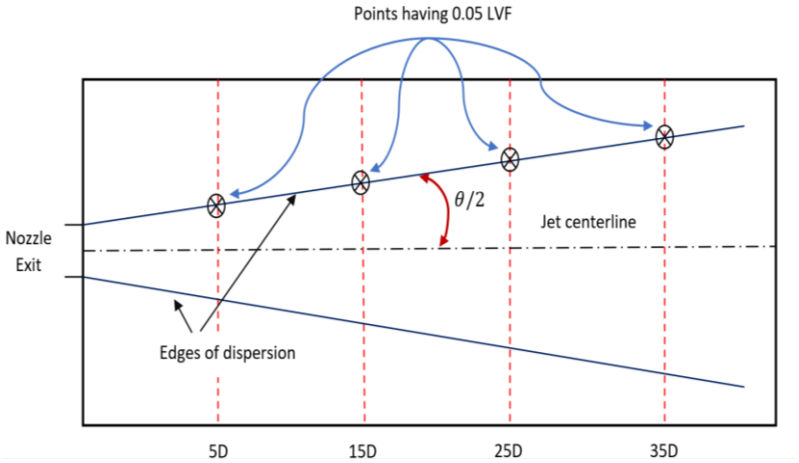

Figure 12 Schematic diagram shows the procedure of obtaining the dispersion angle.

To predict the values of the spray dispersion angle, the boundaries of the jet should be determining first. There are 3 different criteria for defining the jet boundary as reported by Iyer and Abraham [49]. The criterion consistent with Jiang *et al.* [50] was adopted in this work. The criterion states that the boundary is defined as the locus of points having a fixed low value of liquid volume fraction. The specified value of the density is kept the same for all cases. Accordingly, 0.05 was the fixed value of average volume fraction that taken in this work, to bound the liquid jet at different axial distances, then connect these points as illustrated in the schematic diagram shown in **Figure 12**. The locus of points having liquid volume fraction (LVF) of 0.05 were listed in **Table 4**, and located in the upper half of the flow domain as shown in **Figure 13**.

Table 4 Position in y-direction of points having average (LVF) of 0.05.

$\rho_g\ (kg/m^3)$	$Y_{0.05}/D$			
	5d	**15d**	**25d**	**35d**
15	1.18	2.17	2.83	3.46
25	1.37	2.76	3.47	4.23
34.5	1.75	3.61	4.8	4.72

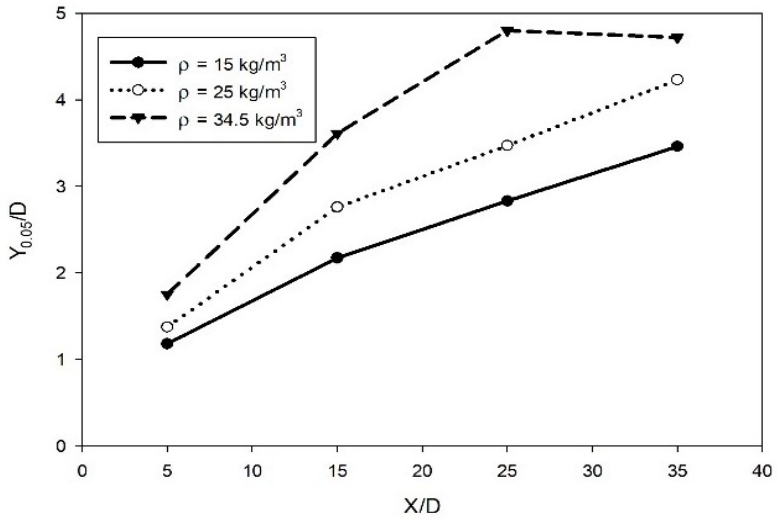

Figure 13 Points having average LVF of 0.05 at different distances for different gas densities.

The calculated dispersion angle for all cases is listed in **Table 5**. From that, it was concluded that the spray dispersion angle is directly proportional to the density. This is consistent with what was observed in the previous section from average liquid volume fraction contours.

Table 5 The calculated cone angles.

$\boldsymbol{\rho_g}$ $(\boldsymbol{kg/m^3})$	$\boldsymbol{\theta}$ $(\boldsymbol{deg.})$
15	12.14
25	15.7
34.5	21.22

Conclusions

In this work, impact of surrounding gas density on the turbulent liquid jet is investigated numerically using LES in ANSYS-FLENT. Validation and grid independency test first performed at different jet velocities. Then the impact of surrounding gas densities is investigated by change the gas density between ρ_g = 15, 25 and 34.5 kg/m^3. It can be concluded that:

1) The decay of average streamwise velocity, u_{avg}, along the jet centerline is the same for the 3 cases (ρ_g= 15, 25 and 34.5 kg/m^3) up to 20D from the nozzle exit, while, from 20D to 40D, a strong decay takes place for highest gas density, and weak decay for the smallest.

2) The density of the ambient gas inversely affects the length of the liquid core, where the core lengths are 24D, 19.1D and 16.2D at gas density of 15, 25 and 34.5 kg/m^3, respectively, indicating that the effect of gas density on the liquid core length is considerably stronger in the gas density range between 15 - 25 kg/m^3 than that in the range of 25 - 34.5 kg/m^3.

3) The spray dispersion angle is directly proportional to the ambient gas density, where the angles are 12.14, 15.7 and 21.22 at gas density of 15, 25 and 34.5 kg/m^3, respectively.

Future scope

In the future, it is intended to extend the current work to 3-dimension simulation with larger number of grid points. Also, more statistics would be investigated such as root-mean-squared of velocity, energy spectrum, etc.

References

[1] N Ashgriz. *Handbook of atomization and sprays*. Springer Science & Business Media, Berlin, Germany, 2011.

[2] MR Morad, M Nasiri and G Amini. Axis-switching and breakup of rectangular liquid jets. *Int. J. Multiphase Flow* 2020; **126**, 103242.

[3] N Odier, G Balarac and C Corre. Numerical analysis of the flapping mechanism for a two-phase coaxial jet. *Int. J. Multiphase Flow* 2018; **106**, 164-78.

[4] H Eroglu and N Chigier. Wave characteristics of liquid jets from airblast coaxial atomizers. *Atomization Sprays* 1991; **1**, 349-66.

[5] F Savart. Me ´moire sur la constitution des veines liquids lance ´es par des orifices circulaires en mince paroi. *Ann. Chem.* 1833 ; **53**, 337-86.

[6] MJ McCarthy and NA Molloy. Review of stability of liquid jets and the influence of nozzle design. *Chem. Eng. J.* 1974; **7**, 1-20.

[7] AH Lefebvre. *Atomization and sprays*. Hemisphere Publishing Corporation, New York, 1989.

[8] N Chigier and RD Reitz. Regimes of jet breakup and breakup mechanisms (physical aspects). *In*: KK Kuo (Ed.). Recent advances in spray combustion: Spray atomization and drop burning phenomena. *Progress in Astronautics and Aeronautics*. American Institute of Aeronautics and Astronautics, Virginia, 1996, p. 109-35.

[9] SP Lin and RD Reitz. Drop and spray formation from a liquid jet. *Ann. Rev. Fluid Mech.* 1998; **30**, 85-105.

[10] C Dumouchel. On the experimental investigation on primary atomization of liquid streams. *Exp. Fluid.* 2008; **45**, 371-422.

[11] H Hiroyasu and T Kadota. Fuel droplet size distribution in diesel combustion chamber. *SAE Tech. Papers* 1974; **83**, 2615-24.
[12] MM Elkotb. Fuel atomization for spray modelling. *Progr. Energ. Combust. Sci.* 1982; **8**, 61-91.
[13] KS Varde, DM Popa and LK Varde. Spray angle and atomization in diesel sprays. *SAE Tech. Papers* 1984; **93**, 779-87.
[14] GM Faeth, LP Hsiang and PK Wu. Structure and breakup properties of sprays. *Int. J. Multiphase Flow* 1995; **21**, 99-127.
[15] RD Reitz and FV Bracco. Mechanism of atomization of a liquid jet. *Phys. Fluids* 1982; **25**, 1730-42.
[16] A Fath. Investigation of the diesel spray break-up close to the nozzle at different injection conditions. *In*: Proceedings of the 4th International Symposium on Diagnostics and Modeling of Combustion in Internal Combustion Engines, Kyoto, Japan. 1998.
[17] A Gupta, H Guo, M Zhai and CN Markides. Primary atomization of liquid-fuel jets in confined turbulent pipe-flows of air at elevated temperatures. *Int. J. Heat Mass Tran.* 2022; **196**, 123285.
[18] C Hotz, M Haas, S Wachter, S Fleck and T Kolb. Experimental investigation on entrainment in two-phase free jets. *Fuel* 2023; **335**, 126912.
[19] A Kumar and S Sahu. Preheated liquid jet breakup dynamics in a twin-fluid injector. *Chem. Eng. Sci.* 2022; **257**, 117723.
[20] S Martínez-Martínez, FA Sánchez-Cruz, JM Riesco-Ávila, A Gallegos-Muñoz and SM Aceves. Liquid penetration length in direct diesel fuel injection. *Appl. Therm. Eng.* 2008; **28**, 1756-62.
[21] HK Suh and CS Lee. Effect of cavitation in nozzle orifice on the diesel fuel atomization characteristics. *Int. J. Heat Fluid Flow* 2008; **29**, 1001-9.
[22] WA Sirignano and C Mehring. Review of theory of distortion and disintegration of liquid streams. *Progr. Energ. Combust. Sci.* 2000; **26**, 609-55.
[23] WD Bachalo. Spray diagnostics for the twenty-first century. *Atomization Sprays* 2000; **10**, 439-74.
[24] DB Barnett, SR Nahorski and EL Rugg. Characteristics of (-)-[3H]-dihydroalprenolol binding to beta-adrenoceptors on rat lung membranes. *Br. J. Pharmacol.* 1977; **61**, 459.
[25] C Tropea and J Foss. *Springer handbook of experimental fluid mechanics*. Springer Berlin, Heidelberg, Germany, 2007.
[26] N Chigier. The Future of Atomization and Sprays. *In*: Proceedings of the 20th Annual Conference on Liquid Atomization and Spray Systems, Orléans, France. 2005.
[27] CW Hirt and BD Nichols. Volume of fluid (VOF) method for the dynamics of free boundaries. *J. Comput. Phys.* 1981; **39**, 201-25.
[28] S Osher and JA Sethian. Fronts propagating with curvature-dependent speed: Algorithms based on Hamilton-Jacobi formulations. *J. Comput. Phys.* 1988; **79**, 12-49.
[29] M Sussman and EG Puckett. A coupled level set and volume-of-fluid method for computing 3D and axisymmetric incompressible two-phase flows. *J. Comput. Phys.* 2000; **162**, 301-37.
[30] T Ménard, S Tanguy and A Berlemont. Coupling level set/VOF/ghost fluid methods: Validation and application to 3D simulation of the primary break-up of a liquid jet. *Int. J. Multiphase Flow* 2007; **33**, 510-24.
[31] S Som, SK Aggarwal, EM El-Hannouny and DE Longman. Investigation of nozzle flow and cavitation characteristics in a diesel injector. *J Eng. Gas Turbines Power* 2010; **132**, 042802.
[32] W Yuan and GH Schnerr. Numerical simulation of two-phase flow in injection nozzles: Interaction of cavitation and external jet formation. *J. Fluids Eng. Trans. ASME* 2003; **125**, 963-9.
[33] M Ghiji, L Goldsworthy, PA Brandner, V Garaniya and P Hield. Numerical and experimental investigation of early stage diesel sprays. *Fuel* 2016; **175**, 274-86.
[34] F Xiao, M Dianat and JJ McGuirk. LES of turbulent liquid jet primary breakup in turbulent coaxial air flow. *Int. J. Multiphase Flow* 2014; **60**, 103-18.
[35] GA Siamas, X Jiang and LC Wrobel. Direct numerical simulation of the near-field dynamics of annular gas-liquid two-phase jets. *Phys. Fluids* 2009; **21**, 042103.
[36] H Grosshans, A Movaghar, L Cao, M Oevermann, RZ Szász and L Fuchs. Sensitivity of VOF simulations of the liquid jet breakup to physical and numerical parameters. *Comput. Fluids* 2016; **136**, 312-23.
[37] J Shinjo and A Umemura. Simulation of liquid jet primary breakup: Dynamics of ligament and droplet formation. *Int. J. Multiphase Flow* 2010; **36**, 513-32.
[38] F Zhang, T Zirwes, S Wachter, T Jakobs, P Habisreuther, N Zarzalis, D Trimis, T Kolb, H Bockhorn and D Stapf. Numerical simulations of air-assisted primary atomization at different air-to-liquid injection angles. *Int. J. Multiphase Flow* 2023; **158**, 104304.

[39] X Leng, Y Deng, W Guan, W Xie, Z He, Q Wang, X Yan and W Long. A numerical study on the in-nozzle cavitating flow and near-field jet breakup of a spirally grooved hole nozzle using a LES-VOF method. *Fuel* 2022; **326**, 125016.
[40] A Abdelsamie and D Thévenin. Direct numerical simulation of spray evaporation and autoignition in a temporally-evolving jet. *Proc. Combust. Inst.* 2017; **36**, 2493-502.
[41] RDC Ward. Current notes on meteorology. *Science* 1906; **23**, 714-5.
[42] F Nicoud and F Ducros. Subgrid-scale stress modelling based on the square of the velocity gradient tensor. *Flow, Turbulence Combust.* 1999; **62**, 183-200.
[43] N Arya and A De. Effect of grid sensitivity on the performance of wall adapting SGS models for LES of swirling and separating-reattaching flows. *Comput. Math. Appl.* 2019; **78**, 2035-51.
[44] Z Pavlovic, S Scheidl, W Edelbauer, B Basara, G Brenn and S Jakirlic. Numerical investigation of the liquid core length in sprays with fully turbulent boundary condition. *In*: Proceedings of the 26th Annual Conference on Liquid Atomization and Spray Systems, Bremen, Germany. 2014.
[45] Ansys. *Ansys fluent user's guide 2020 R1*. Ansys, Pennsylvania, 2020, p. 724-46.
[46] M Arai, M Shimizu and H Hiroyasu. Break-up length and **spray** angle of high speed jets. *In*: Proceedings of the 3rd International Conference on Liquid Atomization and Spray Systems at Imperial College, London, United Kingdom. 1985.
[47] H Hiroyasu, M Shimizu and M Arai. The breakup of high speed jet in a high pressure gaseous atmosphere. *In*: Proceedings of the 2nd International Conference on Liquid Atomization and Spray Systems, ICLASS, Madison, Wisconsin, USA. 1982.
[48] SA Stanley, S Sarkar and JP Mellado. A study of the flow-field evolution and mixing in a planar turbulent jet using direct numerical simulation. *J. Fluid Mech.* 2002; **450**, 377-407.
[49] V Iyer and J Abraham. Penetration and dispersion of transient gas jets and sprays. *Combust. Sci. Tech.* 1997; **130**, 315-34.
[50] Y Jiang, Z Issaka, H Li, P Tang and C Chen. Range formula based on angle of dispersion and nozzle configuration from an impact sprinkler. *Int. J. Agr. Biol. Eng.* 2019; **12**, 97-105.